Electronic, Magnetic, and Redox Properties of $[MFe_3S_4]$ Clusters (M = Cd, Cu, Cr) in *Pyrococcus furiosus* Ferredoxin

Christopher R. Staples,[†] Ish K. Dhawan,[†] Michael G. Finnegan,[†] Derek A. Dwinell,[†] Zhi Hao Zhou,[‡] Heshu Huang,[‡] Marc F. J. M. Verhagen,[‡] Michael W. W. Adams,[‡] and Michael K. Johnson*[,†]

Departments of Chemistry and Biochemistry & Molecular Biology and Center for Metalloenzyme Studies, University of Georgia, Athens, Georgia 30602

Received February 20, 1997[⊗]

The ground- and excited-state properties of heterometallic $[CuFe_3S_4]^{2+,+}$, $[CdFe_3S_4]^{2+,+}$, and $[CrFe_3S_4]^{2+,+}$ cubane clusters assembled in *Pyrococcus furiosus* ferredoxin have been investigated by the combination of EPR and variable-temperature/variable-field magnetic circular dichroism (MCD) studies. The results indicate Cd^{2+} incorporation into $[Fe_3S_4]^{0,-}$ cluster fragments to yield $S = 2$ $[CdFe_3S_4]^{2+}$ and $S = {}^5/_2$ $[CdFe_3S_4]^{+}$ clusters and Cu^{+} incorporation into $[Fe_3S_4]^{+,0}$ cluster fragments to yield $S = {}^1/_2$ $[CuFe_3S_4]^{2+}$ and $S = 2$ $[CuFe_3S_4]^{+}$ clusters. This is the first report of the preparation of cubane type $[CrFe_3S_4]^{2+,+}$ clusters, and the combination of EPR and MCD results indicates $S = 0$ and $S = {}^3/_2$ ground states for the oxidized and reduced forms, respectively. Midpoint potentials for the $[CdFe_3S_4]^{2+,+}$, $[CrFe_3S_4]^{2+,+}$, and $[CuFe_3S_4]^{2+,+}$ couples, $E_m = -470 \pm 15$, -440 ± 10, and $+190 \pm 10$ mV (*vs* NHE), respectively, were determined by EPR-monitored redox titrations or direct electrochemistry at a glassy carbon electrode. The trends in redox potential, ground-state spin, and electron delocalization of $[MFe_3S_4]^{2+,+}$ clusters in *P. furiosus* ferredoxin are discussed as a function of heterometal (M = Cr, Mn, Fe, Co, Ni, Cu, Zn, Cd, and Tl).

Introduction

In addition to their well-established role in mediating electron transfer, there is increasing evidence that iron−sulfur clusters serve a wide variety of functions in biology.[1] They constitute, in whole or in part, the active sites of a variety of redox enzymes, such as nitrogenase,[2] sulfite reductase,[3] carbon monoxide dehydrogenase,[4] and hydrogenase,[5] and nonredox (de)hydratase enzymes, such as aconitase.[6] In order to regulate gene expression or enzyme activity, they appear to act as sensors of iron in the iron responsive protein,[7] oxygen in the fumarate nitrate reduction protein[8] and in glutamine phosphoribosyl pyrophosphate amidotransferase,[9] superoxide in the SoxR protein,[10] and nitric oxide in mammalian ferrochelatase.[11] More recently they have been implicated in coupling proton and electron in nitrogenase,[12] stabilizing a thiyl radical intermediate in ferredoxin−thioredoxin reductase,[13] and possibly generating a radical intermediate in the activating enzymes of anaerobic ribonucleotide reductase and pyruvate formate-lyase,[14] lysine-2,3-aminomutase,[15] and biotin synthase[16] that function by radical mechanisms.

Catalytically active Fe−S clusters have been found to be based on a cubane-type $[Fe_4S_4]$ structural unit that lacks cysteinyl ligation at the specific iron site and/or with a specific iron replaced with another transition metal. Aconitase is the best characterized example of the former, whereas nitrogenase provides an example of the latter type of active site cluster. The potential for heterometallic cubane-type clusters to participate in enzymatic catalysis has, therefore, sparked interest in their reactivity and properties. Holm and co-workers have synthesized and characterized a range of cubane clusters

* Corresponding author. Telephone: 706-542-9378. Fax: 706-542-2353. E-mail: johnson@sunchem.chem.uga.edu.

[†] Department of Chemistry and Center for Metalloenzyme Studies.

[‡] Department of Biochemistry & Molecular Biology and Center for Metalloenzyme Studies.

[⊗] Abstract published in *Advance ACS Abstracts,* November 1, 1997.

(1) (a) Johnson, M. K. In *Encyclopedia of Inorganic Chemistry*; King, R. B., Ed.; Wiley, Chichester, U.K., 1994; Vol. 4, pp 1896−1915. (b) Cammack, R. *Adv. Inorg. Chem.* **1992**, *38*, 281−322.

(2) (a) Kim, J.; Rees, D. C. *Science* **1992**, *257*, 1677−1682. (b) Chan, M. K.; Kim, J.; Rees, D. C. *Science* **1993**, *260*, 792−794.

(3) Crane, B. R.; Siegel, L. M.; Getzoff, E. D. *Science* **1995**, *270*, 59−67

(4) (a) Qiu, D.; Kumar, M.; Ragsdale, S. W.; Spiro, T. G. *Science* **1994**, 817−819. (b) Kumar, M.; Qiu, D.; Spiro, T. G.; Ragsdale, S. W. *Science* **1995**, *270*, 628−630.

(5) Adams, M. W. W. *Biochim. Biophys. Acta* **1990**, *1020*, 115−145.

(6) (a) Beinert, H.; Kennedy, M. C.; Stout, C. D. *Chem. Rev.* **1996**, *96*, 2335−2373. (b) Flint, D. H.; Allen, R. M. *Chem. Rev.* **1996**, *96*, 2315−2334.

(7) (a) Haile, D. J.; Rouault, T. A.; Harford, J. B.; Kennedy, M. C.; Blodin, G. A.; Beinert, H.; Klausner, R. D. *Proc. Natl. Acad. Sci. U.S.A.* **1992**, *89*, 11735−11739. (b) Rouault, T. A.; Klausner, R. D. *TIBS* **1996**, *21*, 174−177.

(8) (a) Khoroshilova, N.; Beinert, H.; Kiley, P. J. *Proc. Natl. Acad. Sci. U.S.A.* **1995**, *92*, 2499−2503. (b) Khoroshilova, N.; Popescu, C.; Münck, E.; Beinert, H.; Kiley, P. J. *Proc. Natl. Acad. Sci. U.S.A.* **1997**, *94*, 6087−6092.

(9) Smith, J. L.; Zaluzec, E. J.; Wery, J.-P.; Niu, L.; Switzer, R. L.; Zalkin, H.; Satow, Y. *Science* **1994**, *264*, 1427−1433.

(10) (a) Wu, J.; Dunham, W. R.; Weiss, B. *J. Biol. Chem.* **1995**, *270*, 10323−10327. (b) Hidalgo, E.; Bollinger, J. M., Jr.; Bradley, T. M.; Walsh, C. T.; Demple, B. *J. Biol. Chem.* **1995**, *270*, 20908−10914. (c) Ding, H.; Hidalgo, E.; Demple, B. *J. Biol. Chem.* **1996**, *271*, 33173−33175.

(11) (a) Dailey, H. A.; Finnegan, M. G.; Johnson, M. K. *Biochemistry* **1994**, *33*, 403−407. (b) Sellers, V. M.; Johnson, M. K.; Dailey, H. A. *Biochemistry* **1996**, *35*, 2699−2704.

(12) Peters, J. W.; Stowell, M. H. B.; Soltis, S. M.; Finnegan, M. G.; Johnson, M. K.; Rees, D. C. *Biochemistry* **1997**, *36*, 1181−1187.

(13) Staples, C. R.; Ameyibor, E.; Fu, W.; Gardet-Salvi, L.; Stritt-Etter, A.-L.; Schürmann, P.; Knaff, D. B.; Johnson, M. K. *Biochemistry* **1996**, *35*, 11425−11434.

(14) (a) Ollagnier, S.; Mulliez, E.; Gaillard, J.; Eliasson, R.; Fontecave, M.; Reichard, P. *J. Biol. Chem.* **1996**, *271*, 9410−9416. (b) Broderick, J. B.; Duderstadt, R. E.; Fernandez, D. C.; Wojtuszewski, K.; Henshaw, T. F.; Johnson, M. K. *J. Am. Chem. Soc.* **1997**, *119*, 77396−77397.

(15) Frey, P. A.; Reed, G. H. *Adv. Enzymol.* **1993**, *66*, 1−39.

(16) (a) Sanyal, I.; Cohen, G.; Flint, D. H. *Biochemistry* **1994**, *33*, 3625−3631. (b) Duin, E. C.; Lafferty, M. E.; Crouse, B. R.; Allen, R. M.; Sanyal, I., Flint, D. H.; Johnson, M. K. *Biochemistry* **1997**, *36*, 11811−11820.

S0020-1669(97)00200-0 CCC: $14.00

containing [MFe_3S_4] cores (M = V, Co, Ni, Nb, Mo, W, Re, Zn, Tl, Cu, Ag),[17] and the ability of biological [Fe_3S_4] clusters to take up exogenous metals has lead to the formation of [MFe_3S_4] clusters in ferredoxins (M = Mn,[18] Co,[18−20] Ni,[20−22] Cu,[23] Zn,[18,22,24,25] Cd,[20,25,26] Ga,[26] Tl[27,28]). These studies have provided insight not only into site specific chemistry at the unique metal sites but also into the valence delocalization and intracluster magnetic interactions of heteronuclear cubane clusters.

Pyrococcus furiosus ferredoxin (*Pf* Fd) is a small hyperthermostable electron transfer protein (M_r = 7500) which contains a single [Fe_4S_4] cluster and undergoes facile [Fe_4S_4] ↔ [Fe_3S_4] interconversion under appropriate experimental conditions due, in large part, to non-cysteinyl coordination at a specific Fe site.[29,30] The removable iron is coordinated by an aspartate,[31,32] which occupies position 14 of the amino acid sequence, corresponding to a ligand arrangement of C-X_2-D-X_2-C-X_{38}-C. Thus far we have characterized the electronic, magnetic, and redox properties of [MFe_3S_4]$^{n+}$ clusters in *Pf* Fd, where M = Mn (n = 1),[18] Fe (n = 1, 2),[29] Co (n = 1, 2),[18] Ni (n = 1),[21,22] Zn (n = 1, 2),[18,22] and Tl (n = 1, 2),[28] and compared them with similar clusters in *Desulfuricans africanus* Fd III (*Da* FdIII),[23,25,27] which also has aspartyl coordination of the removable Fe, and in *Desulfovibrio gigas* Fd II (*Dg* FdII)[19,20,24,26] and *Thermococcus litoralis* Fd (*Tl* Fd),[33] which both have cysteinyl coordination for the removable Fe.

The results reported here extend our ongoing systematic investigation of the electronic, magnetic, and redox properties of heteronuclear cubanes in *Pf* Fd. [$CuFe_3S_4$]$^{2+,+}$ and [$CdFe_3S_4$]$^{2+,+}$ clusters have been prepared in *Pf* Fd and characterized by the combination of EPR, variable-temperature magnetic circular dichroism (VTMCD), and MCD magnetization studies. The results are compared with those obtained for other heterometallic cubane clusters in *Pf* Fd and with those reported for [$CuFe_3S_4$] clusters in *Da* FdIII[23] and [$CdFe_3S_4$] clusters in *Da* FdIII[25] and *Dg* FdII.[20,26] In addition, we present spectroscopic evidence for the formation of a novel [$CrFe_3S_4$]$^{2+,+}$ cluster in *Pf* Fd and report on the ground- and excited-state properties. This is the first example of a [$CrFe_3S_4$] cluster in a synthetic or biological environment and leaves Sc and Ti as the only first-row transition metals that have yet to be incorporated in a heterometallic cubane cluster.

Materials and Methods

Sample Preparation. *Pyrococcus furiosus* was grown and the ferredoxin purified anaerobically in the presence of 2 mM sodium dithionite as previously described.[34] Conversion to the form containing the [Fe_3S_4]$^+$ cluster involved incubating the air-oxidized Fd with a 5-fold excess of potassium ferricyanide and a 10-fold excess of EDTA at room temperature for 30 min, followed by anaerobic Amicon ultrafiltration to remove excess reagents.[29] Sample concentrations were based on EPR spin quantitations of the $S = {}^1/_2$ resonance. All procedures involving the preparation of heterometallic clusters using this starting material were carried out anaerobically in a glovebox (Vacuum Atmospheres) under an Ar atmosphere with <1 ppm O_2.

Samples of *Pf* Fd containing the [$CdFe_3S_4$]$^+$ cluster were prepared by anaerobic addition of a 5-fold stoichiometric excess of $Cd(NO_3)_2 \cdot 4H_2O$ (99.999%, Aldrich Chemical Co.) to the [Fe_3S_4]^0-containing Fd, in 50 mM Tris/HCl buffer, pH 7.8, and in the presence of a 5-fold excess of sodium dithionite. The sample was incubated for 30−50 min prior to freezing for the spectroscopic measurements. Oxidation to the [$CdFe_3S_4$]$^{2+}$ form was accomplished by addition of a slight excess of thionine under anaerobic conditions (thionine addition until the blue color of oxidized thionine persists) or via dye-mediated oxidative redox titrations using ferricyanide as the oxidant. No attempt was made to remove excess Cd^{2+}, since the presence of excess Cd^{2+} stabilized the [$CdFe_3S_4$]$^{2+,+}$ clusters and did not appear to affect the EPR or VTMCD results.

The preparation of [$CuFe_3S_4$]$^{2+,+}$ clusters in *Pf* Fd initially involved anaerobic addition of a stoichiometric amount of $CuSO_4 \cdot 5H_2O$ (99.999%, Aldrich Chemical Co.) to the [Fe_3S_4]^0-containing Fd in 50 mM Tris/HCl buffer, pH 7.8, in the absence of excess sodium dithionite and incubating at room temperature for 15 min. To ensure complete Cu incorporation and reduction to the [$CuFe_3S_4$]$^+$ oxidation state, this was followed by addition of a 3-fold excess of sodium dithionite and one more equivalent of $CuSO_4$. The black precipitate of CuS was removed by centrifugation, and the supernatant was used for spectroscopic and redox experiments on the [$CuFe_3S_4$]$^+$ cluster in *Pf* Fd. The [$CuFe_3S_4$]$^{2+}$-containing form of *Pf* Fd was obtained from this sample via aerobic oxidation by exchanging the buffer four times with the equivalent aerobic buffer using a Centricon with a 3000 MW cut-off (Amicon Corp.).

Samples of *Pf* Fd containing a [$CrFe_3S_4$]$^+$ cluster were prepared by reducing the [Fe_3S_4]$^+$-containing Fd in 100 mM MES buffer, pH 6.0, with a 5-fold excess of $Cr_2(OOCCH_3)_4(H_2O)_2$ dissolved the same buffer and incubating at room temperature for 15 min. The hydrated chromium(II) acetate was prepared and recrystallized as previously described.[35] Excess chromium(II) acetate was not removed from reduced samples, since control experiments indicated that it did not interfere with EPR and VTMCD studies. Oxidation to the [$CrFe_3S_4$]$^{2+}$ state was attempted by addition of a slight excess of thionin under anaerobic conditions (thionin addition until the blue color of oxidized thionin persists), after removal of excess chromium salts via anaerobic Centricon ultrafiltration.

Spectroscopic Measurements. Variable-temperature and variable-field MCD measurements were recorded on samples containing 50% (v/v) glycerol using a Jasco J-500C spectropolarimeter mated to an Oxford Instruments SM4000 split-coil superconducting magnet. The experimental protocols for measuring MCD spectra of oxygen-sensitive samples at fixed temperatures over the range 1.5−300 K with magnetic

(17) (a) Holm, R. H. *Adv. Inorg. Chem.* **1992**, *38*, 1−71. (b) Zhou, J.; Holm, R. H. *J. Am. Chem. Soc.* **1995**, *117*, 11353−11354. (c) Zhou, J.; Raebiger, J. W.; Crawford, C. A.; Holm, R. H. *J. Am. Chem. Soc.* **1997**, *119*, 6242−6250.
(18) Finnnegan, M. G.; Conover, R. C.; Park, J.-B.; Zhou, Z. H.; Adams, M. W. W.; Johnson, M. K. *Inorg. Chem.* **1995**, *34*, 5358−5369.
(19) Moura, I.; Moura, J. J. G.; Münck, E.; Papaefthymiou, V.; LeGall, J. *J. Am. Chem. Soc.* **1986**, *108*, 349−351.
(20) Moreno, C.; Macedo, A. L.; Moura, I.; LeGall, J.; Moura, J. J. G. *J. Inorg. Biochem.* **1994**, *53*, 219−234.
(21) Conover, R. C.; Park, J.-B.; Adams, M. W. W.; Johnson, M. K. *J. Am. Chem. Soc.* **1990**, *112*, 4562−4564.
(22) Srivastava, K. K. P.; Surerus, K. K.; Conover, R. C.; Johnson, M. K.; Park, J.-B.; Adams, M. W. W.; Münck, E. *Inorg. Chem.* **1993**, *32*, 927−936.
(23) Butt, J. N.; Niles, J.; Armstrong, F. A.; Breton, J.; Thomson, A. J. *Nature Struct. Biol.* **1994**, *1*, 427−433.
(24) Surerus, K. K.; Münck, E.; Moura, I.; Moura, J. J. G.; LeGall, J. *J. Am. Chem. Soc.* **1987**, *109*, 3805−3807.
(25) Butt, J. N.; Armstrong, F. A.; Breton, J.; George, S. J.; Thomson, A. J.; Hatchikian, E. C. *J. Am. Chem. Soc.* **1991**, *113*, 6663−6670.
(26) Münck, E.; Papaefthymiou, V.; Surerus, K. K.; Girerd, J.-J. In *Metal Clusters in Proteins*; Que, L., Jr., Ed.; American Chemical Society: Washington, DC, 1988; Vol. 372, pp 302−325.
(27) Butt, J. N.; Sucheta, A.; Armstrong, F. A.; Breton, J.; Thomson, A. J.; Hatchikian, E. C. *J. Am. Chem. Soc.* **1991**, *113*, 8948−8950.
(28) Fu, W.; Telser, J.; Hoffman, B. M.; Smith, E. T.; Adams, M. W. W.; Finnegan, M. G.; Conover, R. C.; Johnson, M. K. *J. Am. Chem. Soc.* **1994**, *116*, 5722−5729.
(29) Conover, R. C.; Kowal, A. T.; Fu, W.; Park, J.-B.; Aono, S.; Adams, M. W. W.; Johnson, M. K. *J. Biol. Chem.* **1990**, *265*, 8533−8541.
(30) Busse, S. C.; La Mar, G. N.; Yu, L.-P.; Howard, J. B.; Smith, E. T.; Zhou, Z. H.; Adams, M. W. W. *Biochemistry* **1992**, *31*, 11952−11962.
(31) (a) Calzolai, L.; Gorst, C. M.; Zhao, Z.-H.; Teng, Q.; Adams, M. W. W.; La Mar, G. N. *Biochemistry* **1995**, *34*, 11373−11384. (b) Calzolai, L.; Zhou, Z. H.; Adams, M. W. W.; La Mar, G. N. *J. Am. Chem. Soc.* **1996**, *118*, 2513−2514.
(32) Telser, J.; Smith, E. T.; Adams, M. W. W.; Conover, R. C.; Johnson, M. K.; Hoffman, B. M. *J. Am. Chem. Soc.* **1995**, *117*, 5133−5140.
(33) Hankins, H. L. M.S. Thesis, University of Georgia, Athens, GA, 1994.
(34) Aono, S.; Bryant, F. O.; Adams, M. W. W. *J. Bacteriol.* **1989**, *171*, 3433−3439.
(35) Ocone, L. R.; Block, B. P. *Inorg. Synth.* **1966**, *8*, 125−130.

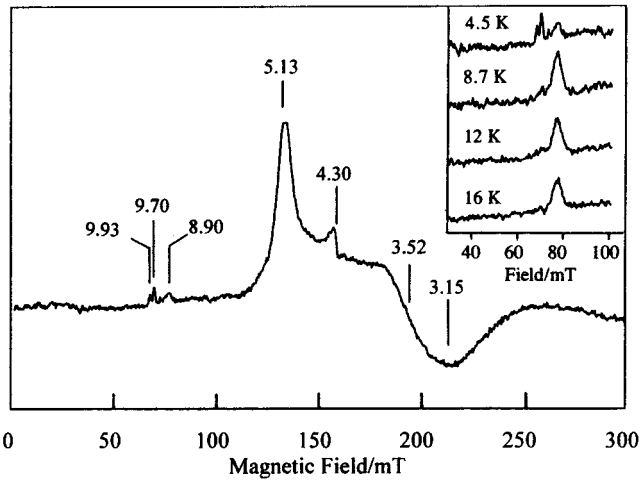

Figure 1. X-band EPR spectrum of the $[CdFe_3S_4]^+$ cluster in dithionite-reduced *Pf* Fd. Sample concentration was 0.2 mM in Fd, and the medium was 50 mM Tris/HCl buffer, pH 7.8, with 1 mM sodium dithionite and 1 mM $Cd(NO_3)_2$. The spectrum was recorded at 4.5 K. Conditions of measurement: microwave power, 100 mW; microwave frequency, 9.60 GHz; modulation amplitude, 0.63 mT. Selected *g*-values are indicated by vertical lines. Inset: Temperature dependence of the low-field region.

fields up to 6 T have been described elsewhere.[36] Variable-temperature (4−30 K), X-band EPR spectra were recorded on a Bruker ESP-300E spectrometer equipped with a ER-4116 dual mode cavity and an Oxford Instruments ESR-9 flow cryostat. Spin quantitations were carried out under nonsaturating conditions using 1 mM CuEDTA as the standard.

Electrochemical Methods. EPR-monitored redox titrations for the $[CdFe_3S_4]^{2+,+}$ cluster were carried at room temperature in the glovebox under anaerobic conditions in 50 mM Tris/HCl buffer, pH 7.8, with a 10-fold excess of Cd^{2+}, using the method described by Dutton.[37] Low-potential mediator dyes were added, each to the concentration of ca. 50 μM, in order to cover the desired range of redox potentials, i.e. methyl viologen, benzyl viologen, neutral red, and safranin O. The reduced cluster was oxidatively titrated with stock solution of potassium ferricyanide. After equilibration at the desired potential, a 250 μL aliquot was transferred to a calibrated EPR tube and immediately frozen in liquid nitrogen. Potentials were measured with a working platinum electrode and a saturated calomel reference electrode and are reported relative to the normal hydrogen electrode (NHE).

Differential pulse and cyclic voltammograms were recorded using a EG&G PAR 264 A polarographic analyzer (Princeton Applied Research) and a three electrode cell as described by Hagen.[38] Samples of 10 μL (0.2−0.3 mM in Fd) were suspended as a drop between a platinum counter electrode, a Ag/AgCl reference electrode, and a polished glassy carbon electrode. Scan rates were in the range 5−10 mV/s, and potentials are reported relative to NHE.

Results

$[CdFe_3S_4]^{2+,+}$ Clusters in *P. furiosus* Fd. Anaerobic incubation of the $[Fe_3S_4]^0$ form of *Pf* Fd with a 5-fold excess of $Cd(NO_3)_2$ in the presence of excess dithionite resulted in partial bleaching of the visible absorption. The absorption changes (not shown) were analogous to those reported for the addition of Zn^{2+}, Co^{2+}, or Mn^{2+} [18] and suggest that the $[Fe_3S_4]^0$ fragment undergoes further reduction on Cd^{2+} incorporation to yield a $[CdFe_3S_4]^+$ cluster.

X-band EPR spectra of the resulting sample, Figure 1, can be readily interpreted as a mixture of two $S = {}^5/_2$ species, and the effective *g*-values of both can be rationalized using an isotropic $S = {}^5/_2$ spin Hamiltonian:

$$H = g_0\beta\mathbf{H}\cdot\mathbf{S} + D[\mathbf{S}_z^2 - S(S+1)/3 + (E/D)(\mathbf{S}_x^2 - \mathbf{S}_y^2)] \quad (1)$$

The major species is responsible for the absorption-shaped features centered at $g = 9.93$ and 8.90 and the dominant component with a near-axial line shape at $g_{x,y,z} = 5.13$, 3.52, and 3.15. On the basis of their temperature-dependence behavior, inset in Figure 1, the $g = 9.93$ and 8.90 features are attributed to the low-field components of resonances from the lower and upper doublets, respectively, with the middle doublet responsible for the dominant axial species. The rhombicity parameter (*E/D*) is estimated as 0.18, since this value predicts three Kramers doublets with effective *g*-values ($g_{x,y,z}$ = (0.23, 0.20, 9.92), (3.51, 3.16, 5.19), and (2.25, 8.95, 1.27) for the ground, middle, and upper doublets, respectively, for $D < 0$ and $g_0 = 2$) very close to the observed values. The energy separation, Δ, between the ground and upper doublets was estimated from the slope of a plot of the logarithm of the ratio of the intensity of the two field resonances ($\log(I_{g=9.93}/I_{g=8.90})$) versus the reciprocal of the temperature, which is a straight line within the experimental error of the measurement of the absolute temperature (data not shown). This leads to $\Delta = 15 \pm 4$ cm^{-1}, which corresponds to $D = -2.3 \pm 0.7$ cm^{-1}. The minor species is more rhombic ($E/D \sim 0.3$) and accounts for the $g = 9.70$ resonance (lower doublet) and most likely the derivative-shaped feature centered at $g = 4.3$ (middle doublet). Such ground-state parameters are characteristic of adventitiously bound Fe^{3+} ion, but such an assignment is unlikely in this case, since the $g = 9.7$ resonance appears under reducing conditions only after the addition of Cd^{2+}. Both the relative amounts and the ground-state parameters for the two $S = {}^5/_2$ $[CdFe_3S_4]^+$ centers are the same within experimental error as those found for the two $S = {}^5/_2$ $[ZnFe_3S_4]^+$ centers in *Pf* Fd.[18]

The close correspondence in the ground-state properties of $[ZnFe_3S_4]^+$ and $[CdFe_3S_4]^+$ clusters in *Pf* Fd also extends to excited-state properties, as evidenced by VTMCD spectra in the visible region, Figure 2a. The spectra of the $[CdFe_3S_4]^+$ center are indistinguishable from those published previously for the $[ZnFe_3S_4]^+$ center in *Pf* Fd.[18] That these electronic transitions arise from the $S = {}^5/_2$ ground state responsible for the EPR signal is demonstrated by saturation magnetization studies at 775 nm, Figure 2b. The data collected at 1.78 K, when only the lowest doublet of the ground-state manifold is significantly populated, are well fit by theoretical data constructed for a predominantly *xy*-polarized transition from a doublet with $g_{\parallel} = 9.9$ and $g_{\perp} = 0.26$,[39] in excellent agreement with the EPR analysis presented above. At higher temperatures, the magnetization data deviate from the theoretical plot due to the population of higher energy doublets within the $S = {}^5/_2$ manifold.

Oxidation of $[CdFe_3S_4]^+$ cluster in *Pf* Fd was attempted by adding 1-μL aliquots of a buffered, anaerobic thionine solution to the dithionite-reduced sample in the presence of a 5-fold excess Cd^{2+} until the blue color of the oxidized thionin persisted. The changes in the EPR properties are consistent with one electron oxidation, loss of $S = {}^5/_2$ $[CdFe_3S_4]^+$ resonances and the concomitant appearance of a broad low-field EPR signal around $g = 16$ that increases in intensity with decreasing temperature down to 4.2 K. This signal sharpens and intensifies in the parallel-mode EPR spectrum, Figure 3b, indicating an

(36) Johnson, M. K. In *Metal Clusters in Proteins*; Que, L., Jr., Ed.; ACS Symposium Series; American Chemical Society: Washington, DC, 1988; Vol. 372, pp 326−342.
(37) Dutton, P. L. *Meth. Enzymol.* **1978**, *54*, 411−435.
(38) Hagen, W. R. *Eur. J. Biochem.* **1989**, *182*, 523−530.
(39) The expressions used to construct theoretical MCD saturation magnetization curves can be found in: Bennett, D. E.; Johnson, M. K. *Biochim. Biophys. Acta* **1987**, *911*, 71−80.

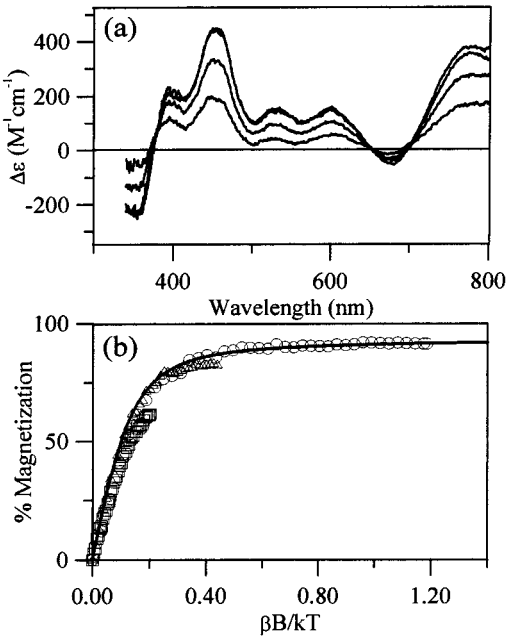

Figure 2. VTMCD spectra and saturation magnetization data for the $[CdFe_3S_4]^+$ cluster in dithionite-reduced *Pf* Fd. The sample was 0.17 mM in Fd and was in 50 mM Tris/HCl buffer, pH 7.8, with 1 mM sodium dithionite and 1 mM $Cd(NO_3)_2$ and 55% (v/v) glycerol. (a) VTMCD spectra with a magnetic field of 6 T at temperatures of 1.78, 4.22, 10.7, and 20.9 K. The intensities of all transitions increase with decreasing temperature. (b) MCD saturation magnetization data collected at 775 nm for magnetic fields between 0 and 6 T with fixed temperatures of 1.78 K (○), 4.22 K (△), 10.7 K (□). The solid line is the theoretical MCD saturation magnetization curve for a transition from an isolated doublet ground state with $g_{\|} = 9.9$, $g_{\perp} = 0.26$, and a polarization ratio $m_z/m_{xy} = -0.2$.

integer-spin ground state.[40] The signal is similar to that observed at $g = 10$ for the $[Fe_3S_4]^0$ cluster in *Pf* Fd, Figure 3a, and is attributed to resonance within the lowest $M_s = \pm 2$ "doublet" of an $S = 2$ ground state with $D < 0$. The shift to lower field for this resonance in $[CdFe_3S_4]^{2+}$ cluster is readily interpreted in terms of greater rhombic splitting within the $M_s = \pm 2$ "doublet" of the $S = 2$ ground state. Moreover, the perturbation of the electronic ground state by incorporation of the heterometal in $[Fe_3S_4]^0$ cluster means that parallel-mode EPR can be used to distinguish between and quantify the amounts of $S = 2$ $[CdFe_3S_4]^{2+}$ and $[Fe_3S_4]^0$ clusters in different preparations. By this criterion, it was established that samples generated by thionine oxidation were 90:10 mixtures of $[CdFe_3S_4]^{2+}$ and $[Fe_3S_4]^0$ clusters, Figure 3b. Samples devoid of the $g = 10$ resonance associated with the $[Fe_3S_4]^0$ cluster were obtained in samples poised at lower potentials (~ -250 mV) in anaerobic dye-mediated redox titrations in the presence of a 10-fold stoichiometric excess of Cd^{2+}. However, the difficulties encountered in obtaining homogeneous samples of the $[CdFe_3S_4]^{2+}$ cluster attest to a much lower Cd^{2+}-binding affinity for the $[Fe_3S_4]^0$ cluster fragment compared to the $[Fe_3S_4]^-$ fragment.

The midpoint potential of $[CdFe_3S_4]^{2+/+}$ couple was determined by dye-mediated EPR redox titrations at pH 7.8 in the presence of a 10-fold stoichiometric excess of Cd^{2+} and using ferricyanide as the oxidant. The intensities of the $g = 5.13$ component of $S = {}^5/_2$ resonance associated with the $[CdFe_3S_4]^+$ cluster (decreases with increasing potential) and the $g = 16$ signal of $S = 2$ $[CdFe_3S_4]^{2+}$ cluster (increases with increasing potential) were monitored in the EPR as a function of potential and fitted to one electron Nernst plots with midpoint potentials of -477 and -465 mV, respectively, Figure 4, indicating a redox potential of -470 ± 15 mV.

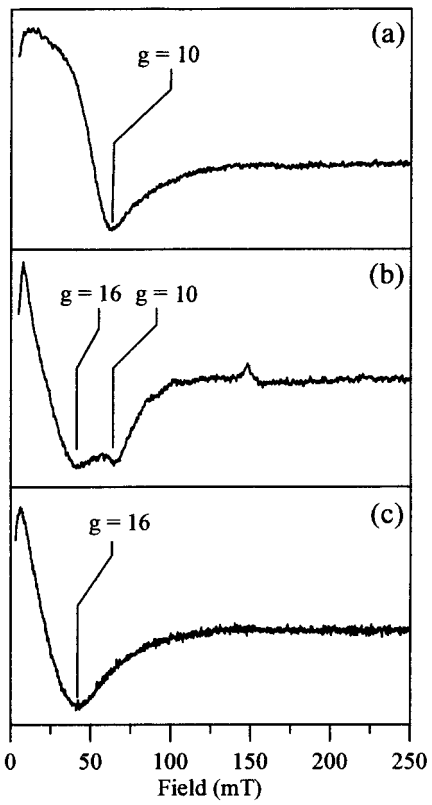

Figure 3. Parallel-mode X-band EPR spectra of $[Fe_3S_4]^0$, $[CdFe_3S_4]^{2+}$, and $[CuFe_3S_4]^+$ clusters in *Pf* Fd. (a) $[Fe_3S_4]^0$ cluster. The sample was 0.25 mM in Fd and was in 50 mM Tris/HCl buffer, pH 7.8, with 1 mM sodium dithionite. (b) $[CdFe_3S_4]^{2+}$ cluster. The sample was 0.20 mM in Fd and was in 50 mM Tris/HCl buffer, pH 7.8, with 1 mM $Cd(NO_3)_2$ and was prepared by thionine oxidation of the dithionite-reduced $[CdFe_3S_4]^+$ cluster. The feature at $g = 10$ is attributed to $[Fe_3S_4]^0$ centers formed by partial loss of Cd^{2+} from the oxidized cluster. (c) $[CuFe_3S_4]^+$ cluster. The sample was 0.33 mM in Fd and was in 50 mM Tris/HCl buffer, pH 7.8, with 1 mM sodium dithionite. Conditions of measurement: microwave power, 10 mW; temperature, 4 K; modulation amplitude, 0.63 mT; microwave frequency, 9.34 GHz.

VTMCD studies of the $[CdFe_3S_4]^{2+}$ cluster in *Pf* Fd were carried out for a sample poised at -277 mV *vs* NHE (sample taken from dye-mediated redox titration) in the presence of 50% (v/v) glycerol. This sample showed no indication of the presence of $[Fe_3S_4]^0$ clusters as evidenced by the absence of the $g = 10$ parallel-mode EPR signal. The VTMCD spectra of the $[Fe_3S_4]^0$ and $[CdFe_3S_4]^{2+}$ clusters in *Pf* Fd are compared in Figure 5a,b. Although the data for the $[CdFe_3S_4]^{2+}$ cluster is of poorer quality due to the lower sample concentration and a birefringent strain in the frozen glass that accounts for the high-frequency oscillations, the spectra clearly show marked similarities. The major differences lie in the loss of the pronounced negative band at $\sim$550 nm and a shift of the intense positive band centered at 700 nm to 750 nm with Cd^{2+} incorporation. As discussed below, both of these changes are likely to reflect perturbation of the Fe−Fe interaction within the valence-delocalized pair of the $[Fe_3S_4]^0$ fragment. The similarity in the excited-state properties of the $[Fe_3S_4]^0$ and $[CdFe_3S_4]^{2+}$ extends to the ground-state properties as revealed by MCD saturation studies. The MCD magnetization properties for the $[CdFe_3S_4]^{2+}$ cluster at 750 nm, Figure 6a, are indistinguishable from those reported for the $[Fe_3S_4]^0$ cluster at 700 nm,[29] and the lowest

(40) (a) Hagen, W. R. *Biochim. Biophys. Acta* **1982**, *708*, 82−98. (b) Hendrich, M. P.; Debrunner, P. G. *J. Magn. Reson.* **1988**, *78*, 133−141. (c) Hendrich. M. P.; Debrunner, P. G. *Biophys. J.* **1989**, *56*, 489−506.

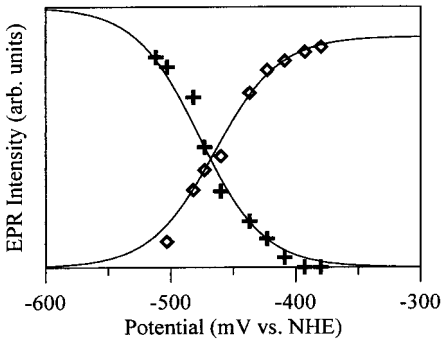

Figure 4. Dye-mediated, oxidative redox titration for the $[CdFe_3S_4]^{2+/+}$ cluster in *Pf* Fd. The EPR intensities of the $g = 5.13$ component (+) of the $S = {}^5/_2$ $[CdFe_3S_4]^+$ cluster (measured at 4.5 K with 50-mW microwave power) and the $g = 16$ resonance (◇) of the $S = 2$ $[CdFe_3S_4]^{2+}$ cluster (measured at 4.5 K with 50-mW microwave power) are plotted are a function of increasing potential (*vs* NHE). The solid lines are the best fits to a one-electron Nernst plot with midpoint potentials of −477 mV for loss of the $g = 5.13$ component and −465 mV for the appearance of the $g = 16$ resonance. The sample was 0.15 mM in Fd and was in 50 mM Tris/HCl buffer, pH 7.8, with 1.5 mM $Cd(NO_3)_2$, and the redox titration was carried out as described in Materials and Methods.

temperature data are well fit by theoretical data constructed for an *xy*-polarized transition from a doublet state with $g_{||} = 8.0$ and $g_\perp = 0.0$. These are the effective g values for a $M_s = \pm 2$ doublet of a $S = 2$ spin state, indicating a $S = 2$ ground state with $D < 0$, in accord with EPR analysis (*vide supra*). Overall the properties of the $[CdFe_3S_4]^{2+}$ cluster are in accord with one electron oxidation of the Fe−S fragment to the $[Fe_3S_4]^0$ core oxidation state, and the minor perturbations in the ground- and excited-state properties are attributed to the presence of Cd^{2+} at the corner of the cube. Very similar VTMCD properties have been observed for the $[ZnFe_3S_4]^{2+}$ cluster in *Pf* Fd[18] and the $[ZnFe_3S_4]^{2+}$ and $[CdFe_3S_4]^{2+}$ clusters in *Da* FdIII.[25]

$[CuFe_3S_4]^{2+,+}$ Clusters in *P. furiosus* Fd. Successful attempts to prepare heterometallic clusters with a $[CuFe_3S_4]$ core in *Pf* Fd involved reducing the $[Fe_3S_4]^{+,0}$ cluster with a minimal amount of sodium dithionite (as monitored by UV−visible absorption) and incubation with a stoichiometric amount of Cu^{2+}. Spectroscopic studies indicated little or no Cu incorporation in preparations involving excess dithionite. Once formed, the cluster was readily reduced to the $[CuFe_3S_4]^+$ level with excess dithionite, and subsequent aerobic oxidation yielded the $[CuFe_3S_4]^{2+}$ cluster. The redox-induced changes in UV−visible absorption for the $[CuFe_3S_4]^{2+,+}$ couple (data not shown) paralleled those observed for the $[Fe_3S_4]^{+,0}$ couple in *Pf* Fd,[18] suggesting a formulation involving Cu^+ bound to a $[Fe_3S_4]^{+,0}$ cluster fragment.

The properties of the putative $[CuFe_3S_4]^+$ cluster in *Pf* Fd were investigated by a combination of EPR and VTMCD spectroscopies. The X-band EPR spectrum of the dithionite-reduced $[CuFe_3S_4]^+$ cluster exhibits a single broad resonance at $g = 16.0$ that sharpens and intensifies in the parallel-mode EPR spectrum, Figure 3c. The signal is indistinguishable from that observed for the oxidized $[CdFe_3S_4]^{2+}$ cluster, Figure 3b, and is likewise attributed to a resonance within the $M_s = \pm 2$ levels of a $S = 2$ ground state with $D < 0$. The absence of the $g = 10$ resonance of the $[Fe_3S_4]^0$ cluster indicates complete Cu incorporation. These ground-state properties and the presence of a homogeneous $[CuFe_3S_4]^+$ in dithionite-reduced preparations were confirmed by VTMCD studies. The VTMCD spectra, Figure 5c, are quite distinctive compared to those exhibited by either the $[CdFe_3S_4]^{2+}$ or $[Fe_3S_4]^0$ clusters in *Pf* Fd but very similar to that reported for the $[CuFe_3S_4]^+$ cluster in *Da* FdIII.[23] Clearly Cu^+ incorporation has a pronounced effect on the

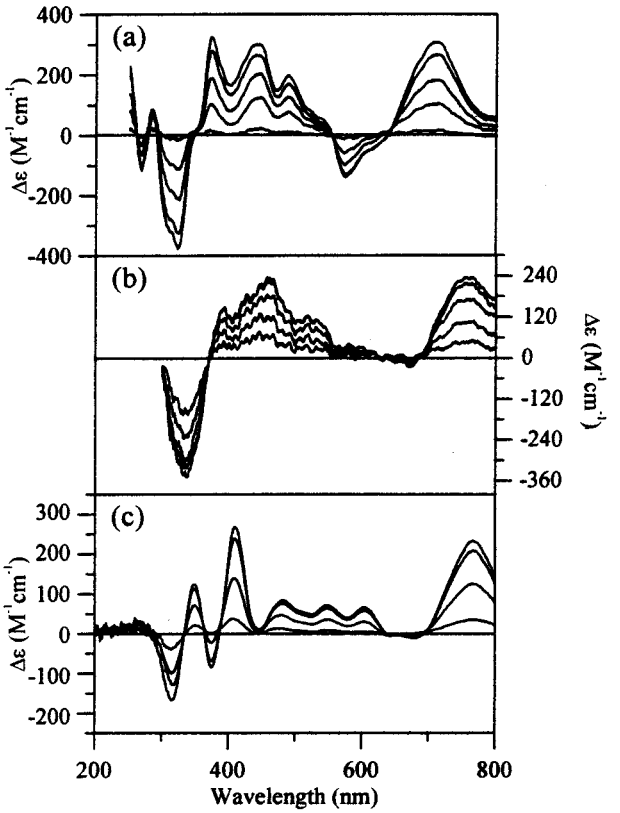

Figure 5. VTMCD spectra of $[Fe_3S_4]^0$, $[CdFe_3S_4]^{2+}$, and $[CuFe_3S_4]^+$ clusters in *Pf* Fd. (a) $[Fe_3S_4]^0$ cluster. The sample, 0.25 mM in Fd, is as described in Figure 3a except for the addition of 50% (v/v) glycerol. The MCD spectra were recorded with a magnetic field of 4.5 T at temperatures of 1.67, 4.22, 9.0, 15.8, and 51.0 K. (b) $[CdFe_3S_4]^{2+}$ cluster. The sample, poised at −277 mV, was taken from the dye-mediated redox titration shown in Figure 5 and diluted with 50% (v/v) glycerol to give a sample concentration of 0.07 mM. MCD spectra were recorded with a magnetic field of 6 T at temperatures of 1.79, 4.22, 10.95, 20.7, and 51.2 K. (c) $[CuFe_3S_4]^+$ cluster. The sample, 0.35 mM in Fd, is as described in Figure 3c except for the addition of 50% (v/v) glycerol. MCD spectra were recorded with a magnetic field of 4.5 T at temperatures of 1.77, 4.22, 9.8, and 51 K. For all three samples, the intensities of the transitions increase with decreasing temperature.

excited-state properties of the $[Fe_3S_4]^0$ cluster, notably a shift in the band at 700 nm to 780 nm and marked changes in higher energy region > 450 nm presumably resulting from the presence of Cu(I) → S charge transfer transitions. However, MCD saturation magnetization studies at 780 nm reveal very similar ground-state properties, Figure 6b. As for the $[CdFe_3S_4]^{2+}$ and $[Fe_3S_4]^0$ clusters in *Pf* Fd, the lowest temperature data are well fit by theoretical data constructed for an *xy*-polarized transition from a doublet state with $g_{||} = 8.0$ and $g_\perp = 0.0$, indicating an $S = 2$ ground state with $D < 0$.

The $[CuFe_3S_4]^{2+,+}$ cluster is unusual compared to other heterometallic clusters in *Pf* Fd in that it is robust enough to be oxidized via exchange into an aerobic Tris/HCl buffer over the course of several hours. X-band EPR spectra of the oxidized $[CuFe_3S_4]^{2+}$ cluster prepared in this way are shown in Figure 7. The spectrum obtained at 4.2 K, thick line in Figure 7a, is dominated by a fast-relaxing resonance, $g_{||} = 2.035$ and $g_\perp \sim 1.94$, that is only observable below 20 K and has relaxation properties and g-values very similar to those of the $[Fe_3S_4]^+$ cluster in *Pf* Fd ($g_{||} = 2.02$ and $g_\perp \sim 1.95$). In addition there is a slower relaxing resonance from adventitiously bound Cu^{2+} (d^9, $S = {}^1/_2$, $I = {}^3/_2$) that is strongly saturated at 4.2 K but persists at 30 K, thin line in Figure 7a. Spin quantitations indicate that contaminating Cu^{2+} is present at a level corresponding to ∼40% of the $[CuFe_3S_4]^+$ concentration, but it can be almost completely

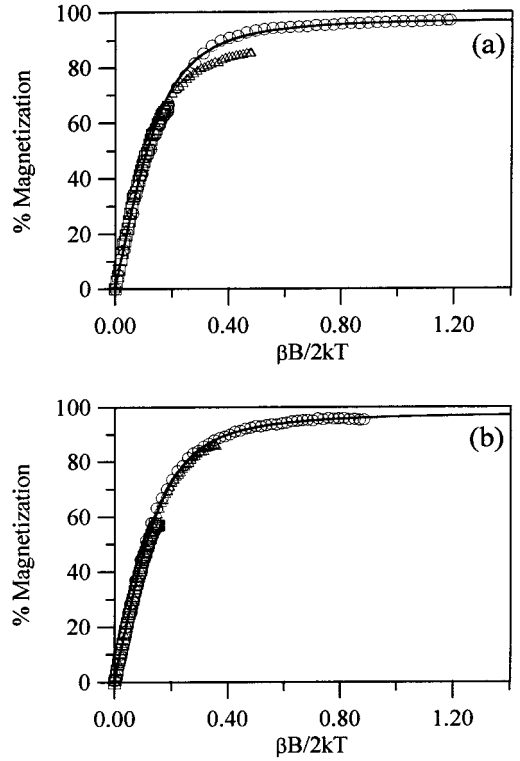

Figure 6. MCD saturation magnetization data for the $[CdFe_3S_4]^{2+}$ and $[CuFe_3S_4]^{+}$ clusters in *Pf* Fd. (a) Saturation magnetization data for the $[CdFe_3S_4]^{2+}$ cluster at 750 nm for magnetic fields between 0 and 6 T and fixed temperatures of 1.79 K (○), 4.22 K (△), and 10.95 K (□). (b) Saturation magnetization data for the $[CuFe_3S_4]^{1+}$ cluster at 780 nm for magnetic fields between 0 and 4.5 T and at fixed temperatures of 1.77 K (○), 4.22 K (△), and 9.79 K (□). The samples are described in Figure 5, and in both cases, the solid lines are theoretical saturation magnetization curves for an *xy*-polarized transition originating from an isolated doublet ground state with $g_{\|} = 8.0$ and $g_{\perp} = 0.00$.

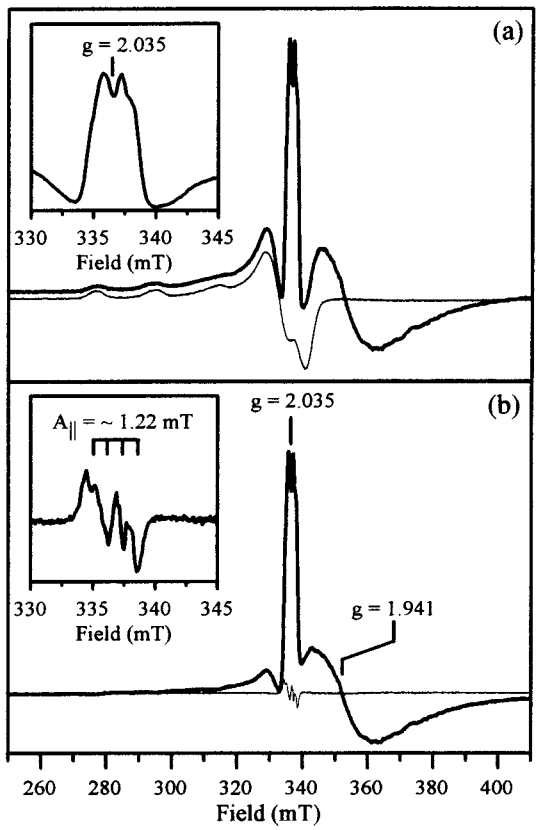

Figure 7. X-band EPR spectra of the $[CuFe_3S_4]^{2+}$ cluster in *Pf* Fd. The sample was 0.30 mM in Fd and was in an aerobic 50 mM Tris/HCl buffer, pH 7.8. (a) EPR spectra at 4.2 K (bold trace) and 30 K (thin trace) recorded with a microwave power of 1.0 mW, a modulation amplitude of 0.63 mT and at a microwave frequency of 9.60 GHz. Inset: Expansion of the sharp feature centered at $g = 2.035$ in the EPR spectrum recorded at 4.2 K. (b) The bold trace is the resultant EPR spectrum after subtraction of the 30 K EPR spectrum (thin trace in A) from the 4.2 K EPR spectrum (bold trace in A). The thin trace is the second derivative EPR spectrum of the bold spectrum. Inset: Expansion of the second derivative EPR spectrum centered around $g = 2.035$.

removed from the observed spectrum by subtracting the 30 K spectrum from the 4.2 K spectrum, thick line in Figure 7b. The residual Cu^{2+} EPR features in Figure 7b are the result of power-saturation broadening of the Cu^{2+} resonance at 4.2 K. Strong evidence for Cu^{+} binding to the trigonal μ_2-S^{2-} face of the $[Fe_3S_4]^{+}$ cluster comes from the observation of resolved[63,65] Cu hyperfine on the $g = 2.035$ component, inset in Figure 7a. This is most readily apparent in the second derivative spectrum, thin line and inset in Figure 7b, and the hyperfine coupling constant is estimated as 1.2 mT. Although this coupling constant is at least 1 order of magnitude less than that typically encountered in Cu^{2+} centers, it demonstrates that the unpaired spin associated the $[Fe_3S_4]^{+}$ fragment is delocalized to a small extent onto the Cu atom. Butt *et al.* have reported a similar EPR spectrum for the $[CuFe_3S_4]^{2+}$ cluster in *Da* FdIII, but no resolved copper hyperfine splitting was observed.[23]

Further evidence that Cu remains bound to cluster after oxidation comes from the VTMCD data. Figure 8 shows a comparison of the VTMCD spectra of the $[Fe_3S_4]^{+}$ and $[CuFe_3S_4]^{2+}$ clusters in *Pf* Fd and MCD magnetization data for the $[CuFe_3S_4]^{2+}$ sample. The latter demonstrates that the electronic transitions originate from the $S = {}^1/_2$ ground state that is responsible for the EPR resonance discussed above. Both samples exhibit complex MCD spectra with numerous positive and negative transitions throughout the UV/visible/near-IR region, but the distinctive nature of each spectra indicates little, if any, residual $[Fe_3S_4]^{+}$ clusters in the $[CuFe_3S_4]^{2+}$ sample. A VTMCD spectrum very similar to that shown in Figure 8b has also been reported for the $[CuFe_3S_4]^{2+}$ clusters in *Da* FdIII. It is interesting to note that, with the exception of the intense positive, negative, positive bands at 408, 370, and 326 nm, respectively, in the $[CuFe_3S_4]^{2+}$ sample, all the lower energy bands have a counterpart in the $[Fe_3S_4]^{+}$ spectrum, with the same sign but shifted up energy by 4000 ± 500 cm^{-1}. This is consistent with assignment of lower energy band to S → Fe(III) charge transfer and the three higher energy bands to Cu(I) → S charge transfer in the $[CuFe_3S_4]^{2+}$ sample. In accord with this assignment, the three Cu(I) → S charge transfer transitions are also observed in the $[CuFe_3S_4]^{+}$ spectrum with the same signs but slightly higher wavelengths, 412, 377, and 350 nm; *vide supra*.

The redox potential of the $[CuFe_3S_4]^{2+,+}$ couple in *Pf* Fd in 50 mM Tris/HCl buffer at pH 7.8 was determined by cyclic voltammetry and differential pulse voltammetry at a glassy carbon electrode. The cyclic voltammograms reveal a quasi-reversible wave with a 92-mV peak-to-peak separation, centered at $+190 \pm 10$ mV, that persisted unchanged through at least 10 redox cycles. Differential pulse voltammetry gave a peak-to-peak separation of 16 mV and a midpoint potential of $+192 \pm 10$ mV, in excellent agreement with the cyclic voltammetry. Hence the electrochemical results confirm that the $[CuFe_3S_4]^{2+,+}$ couple is stable with respect to redox cycling in the absence of excess Cu and indicate a midpoint potential of 190 ± 10 mV.

$[CrFe_3S_4]^{2+,+}$ Clusters in *P. furiosus* Fd. Anaerobic reduction of the $[Fe_3S_4]^{+}$ cluster in *Pf* Fd with a 5-fold excess of chromium(II) acetate at pH 6 resulted in absorption changes

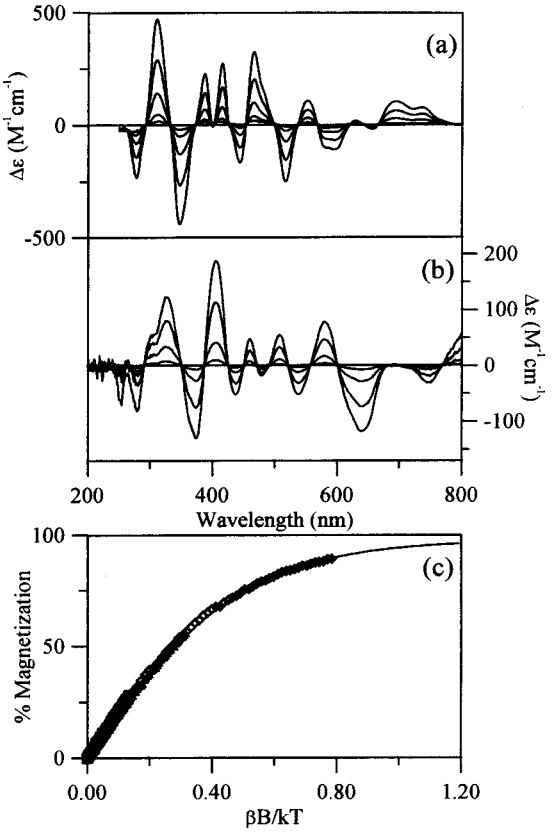

Figure 8. VTMCD spectra of $[Fe_3S_4]^+$ and $[CuFe_3S_4]^{2+}$ clusters in *Pf* Fd. (a) $[Fe_3S_4]^+$ cluster. The sample was 0.25 mM in Fd, and the medium was 50 mM Tris/HCl buffer, pH 7.8, with 50% (v/v) glycerol. The MCD spectra were recorded with a magnetic field of 4.5 T at temperatures of 1.59, 4.22 9.9, 17.6, and 53 K. MCD intensity at all wavelengths increases with decreasing temperature. (b) $[CuFe_3S_4]^{2+}$ cluster. The sample was 0.32 mM in Fd in an aerobic 50 mM Tris/HCl buffer, pH 7.8 with 60% (v/v) polyethylene glycol (MW ~ 200 Da). The MCD spectra were recorded with a magnetic field of 4.5 T at temperatures of 1.70, 4.22, 10.0, and 32 K. (c) MCD saturation magnetization data for the $[CuFe_3S_4]^{2+}$ cluster at 640 nm for magnetic fields between 0 and 4.5 T and at fixed temperatures of 1.70 (◇), 4.22 (△), and 10.0 K (□). The solid line is the theoretical magnetization curve for a transition from an isolated $S = {}^1/_2$ ground state with $g_{\|} = 2.035$, $g_{\perp} = 1.941$, and a polarization ratio $m_z/m_{xy} = -0.3$.

analogous to those associated with the formation of $[MFe_3S_4]^+$ clusters where M = Zn, Mn, Co, or Cd.[18] Additional evidence for the formation of a novel $[CrFe_3S_4]^+$ cluster comes from the unique EPR and VTMCD properties compared to other heterometallic or homometallic cluster in *Pf* Fd.

The EPR spectrum of the sample as prepared at pH 6, Figure 9, can be readily rationalized as a $S = {}^3/_2$ species using the spin Hamiltonian in eq 1. The spectrum is dominated by absorption-shaped features at $g = 5.76$ and 5.06, and temperature-dependence studies over the range 3.8−10 K indicate that these features originate from the upper and lower doublets, respectively, of the ground-state manifold. This indicates $E/D = 0.21$ and $D > 0$, which predicts $g_{x,y,z} = 1.76$, 5.06, 2.70 and 5.76, 1.06, 1.31 for the lower and upper doublets using eq 1 with $g_0 = 2$. In accord with this analysis, weak derivative-shaped features are apparent centered at $g = 2.70$ and 1.31 and a negative absorption-shaped band is discernible at $g = 1.76$. The energy separation between these doublets, Δ, was estimated as 0.78 ± 0.05 cm^{-1} from the slope of a plot of the logarithm of the ratio of the intensities at $g = 5.76$ and 5.06 as a function of the reciprocal temperature, inset in Figure 9. The value of D is estimated at $+0.37 \pm 0.03$ cm^{-1} using the relationship $\Delta = 2D(1 + 3(E/D)^2)^{1/2}$.[41]

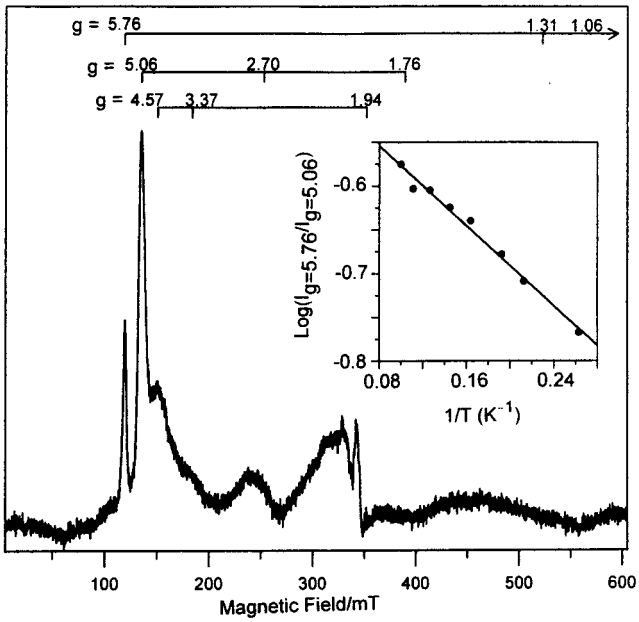

Figure 9. X-band EPR spectrum of the $[CrFe_3S_4]^+$ cluster in *Pf* Fd. The sample, 0.2 mM in Fd, was prepared by adding 1.0 mM $Cr_2(OOCCH_3)_4(H_2O)_2$ to the $[Fe_3S_4]^+$ cluster under strictly anaerobic conditions in 100 mM MES/HCl buffer at pH 6.0. Spectrum was recorded at 9 K. Conditions of measurement: microwave power, 10 mW; microwave frequency, 9.58 GHz; modulation amplitude, 0.63 mT. Features not marked with *g*-values in the $g = 2$ region arise from cavity impurities Inset: Plot of the natural logarithm of the ratio of the intensities at $g = 5.76$ and 5.06 *versus* the inverse of the temperature.

Some preparations also exhibited a more axial $S = {}^3/_2$ species with $g = 4.57$, 3.37, and 1.94. While the factors determining the relative amounts of these two $S = {}^3/_2$ species are still under investigation, the more axial species was difficult to discern (as in Figure 9) except in samples treated with sodium dithionite, when it becomes the dominant resonance (data not shown). The *g*-values and temperature dependence are consistent with $E/D = 0.10$ and $D > 0$ (predicts $g_{x,y,z} = 1.94$, 4.56, 3.38 and 5.94, 0.56, 0.62 for the lower and upper doublets, respectively for $g_0 = 2$) and a weak feature at $g = 5.96$ was apparent at temperatures > 6 K. Control experiments in which Cr^{3+} salts were added to the *Pf* Fd apoprotein and buffer solution used in this work indicate that neither of these $S = {}^3/_2$ species can be attributed to free or protein-bound Cr^{3+} arising from the oxidation of chromium(II) acetate.

VTMCD spectra and saturation magnetization data were obtained for a sample of $[CrFe_3S_4]^+$ *Pf* Fd at pH 6.0 in the presence of 60% (v/v) glycerol, Figure 10. The EPR spectrum was unchanged by the addition of glycerol. The observation of temperature-dependent MCD bands throughout the UV/visible/near-IR region confirms the presence of a paramagnetic Fe−S cluster. However, the spectrum is different from that observed for any paramagnetic homometallic or heterometallic cluster in *Pf* Fd, i.e. $[Fe_3S_4]^{+,0}$,[29] $[Fe_4S_4]^+$,[29] $[ZnFe_3S_4]^{2+,+}$,[18] $[CoFe_3S_4]^{2+,+}$,[18] $[TlFe_3S_4]^{2+,+}$,[28] $[NiFe_3S_4]^+$,[42] $[CdFe_3S_4]^{2+,+}$, Figures 2a and 5b, and $[CuFe_3S_4]^{2+,+}$, Figures 5c and 8b. The overall pattern of positive and negative bands is, however, most similar to that observed for the $[Fe_4S_4]^+$, $[CoFe_3S_4]^+$, and $[NiFe_3S_4]^+$ clusters in *Pf* Fd and $S = {}^3/_2$ $[Fe_4S_4]^+$ clusters in other proteins,[43] indicating that Cr has been incorporated into a heterometallic cubane cluster. The MCD saturation magnetiza-

(41) Hoffman, B. M.; Weschler, C. J.; Basola, F. *J. Am. Chem. Soc.* **1976**, *98*, 5473−5482.
(42) Conover, R. C. Ph.D. Thesis, University of Georgia, Athens, GA, 1993.

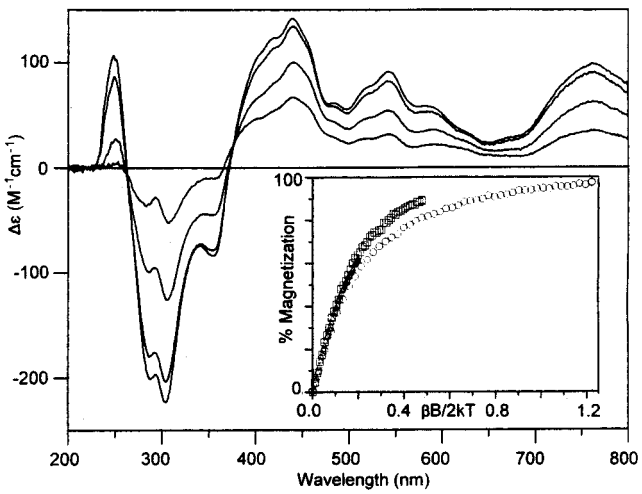

Figure 10. VTMCD spectra and saturation magnetization data for the $[CrFe_3S_4]^+$ cluster in *Pf* Fd. The final sample concentration was 0.16 mM in Fd, and the sample was prepared adding 0.8 mM $Cr_2(OOCCH_3)_4(H_2O)_2$ to the $[Fe_3S_4]^+$ cluster under strictly anaerobic conditions in 100 mM MES/HCl buffer at pH 6.0, followed by the addition of 60% (v/v) glycerol. VTMCD spectra were recorded with a magnetic field of 6 T at temperatures of 1.68, 4.22, 10.2, and 19.9 K. The intensities of all transitions increase with decreasing temperature. The inset shows MCD saturation magnetization data collected at 760 nm for magnetic fields between 0 and 6 T with fixed temperatures of 1.68 (○), 4.22 (□), 10.2 K (△).

tion data collected at 760 nm are also very similar those reported for $S = {}^3/_2$ $[Fe_4S_4]^+$ clusters,[29,43] with data collected at different temperatures lying on separate curves due to the Boltzmann population and/or the field-induced mixing of the zero-field components of the ground-state manifold. The small zero-field splitting complicates the data analysis, and more detailed interpretation in terms of the ground-state parameters has not been attempted thus far.

Attempts to oxidize the cluster to the $[CrFe_3S_4]^{2+}$ state involved anaerobic oxidation with a slight excess of thionine at pH 6.0 after removal of excess chromium salts via Centricon ultrafiltration. The resulting samples were investigated by EPR and VTMCD and found to exhibit the characteristic features associated with $S = {}^1/_2$ $[Fe_3S_4]^+$ clusters.[28] However, the intensity of the MCD spectrum and the EPR spin quantitation indicated that only 10% of these clusters were responsible for these spectroscopic features. Since no additional EPR or temperature-dependent MCD bands were observed, we conclude that the bulk of the clusters have a diamagnetic state, $S = 0$, ground state. Hence, it seems likely that the $[CrFe_3S_4]^{2+}$ clusters has a $S = 0$ ground state that is not amenable to EPR or VTMCD studies. Lower affinity of the oxidized cluster for the heterometal is presumably responsible for the partial degradation to give $[Fe_3S_4]^+$ clusters.

The redox potential of the $[CrFe_3S_4]^{2+,+}$ couple in *Pf* Fd in 50 mM Mops buffer at pH 7.0 was determined by cyclic voltammetry at a glassy carbon electrode. The sample used for these electrochemical experiments was identical to that used for the EPR studies in Figure 9, except that excess chromium salts were removed and the buffer was exchanged by anaerobic Centricon ultrafiltration. The resulting sample showed two quasi-reversible waves centered at -340 ± 10 mV (50 mV peak-to-peak separation) and -440 ± 10 mV (60 mV peak-to-peak separation) in cyclic voltammograms. However, in successive scans, the amplitude of the lower potential wave progressively decreased (almost completely gone after 10 scans) and this was accompanied by a small increase in the amplitude of the −340-mV wave and the appearance of a reversible wave centered at −160 mV. Since the midpoint potentials of the $[Fe_4S_4]^{2+,+}$ and $[Fe_3S_4]^{+,0}$ couples in *Pf* Fd are −345 and −160 mV, respectively,[18] and the EPR experiments reported above indicate that Cr is readily lost on oxidation, these redox results are interpreted in terms of partial conversion to $[Fe_4S_4]^{2+,+}$ clusters during buffer exchange to remove of excess Cr and progressive oxidative loss of Cr during redox cycling to yield $[Fe_3S_4]^{+,0}$ clusters that are capable of scavenging Fe to form additional $[Fe_4S_4]^{2+,+}$ clusters. Hence the redox process with a midpoint potential of -440 ± 10 mV is attributed to the $[CrFe_3S_4]^{2+,+}$ couple.

Discussion

Removal of the non-cysteinyl-coordinated Fe from the $[Fe_4S_4]$ cluster in *Pf* Fd exposes a tri-μ_2-sulfido face to which numerous metals can be incorporated to form heterometallic cubanes. In this work, three additional heterometallic cubane clusters involving $[CdFe_3S_4]^{2+,+}$, $[CuFe_3S_4]^{2+,+}$, and $[CrFe_3S_4]^{2+,+}$ cores have been assembled in *Pf* Fd and characterized in terms of their ground-state, excited-state, and redox properties. With these three clusters, nine heterometallic or homometallic cubanes, $[MFe_3S_4]$, where M = Cr, Mn, Fe, Co, Ni, Cu, Zn, Cd, and Tl, have now been assembled and characterized in *Pf* Fd. This is many more than in any other protein and allows for meaningful examination of the trends in cluster properties as function of the heterometal. Before discussion of such trends, the properties of each of the clusters reported in this work are briefly discussed in light of the available data for analogous clusters in other proteins or clusters in *Pf* Fd with similar ground- and excited-state properties.

$[CdFe_3S_4]^+$ clusters were first assembled in *Dg* FdII and characterized as having $S = {}^5/_2$ ground states on the basis of EPR and Mössbauer studies.[26] Subsequent studies of *Da* FdIII reported a broad unresolved EPR signal in the $g = 4-5$ region that was attributed to the $S = {}^5/_2$ $[CdFe_3S_4]^+$ cluster and EPR and VTMCD evidence for a $S = 2$ $[CdFe_3S_4]^{2+}$ cluster.[25] While the ability to obtain homogeneous preparations of $[CdFe_3S_4]^{2+,+}$ clusters in *Pf* Fd in both oxidation states has allowed more detailed characterization of the ground- and excited-state properties, it is clear that these clusters exhibit very similar properties in all three proteins. Moreover, on the basis of the EPR and VTMCD properties, it is not possible to distinguish between $[ZnFe_3S_4]^{2+}$ and $[CdFe_3S_4]^{2+}$ or $[ZnFe_3S_4]^+$ and $[CdFe_3S_4]^+$ clusters in *Pf* Fd, despite the large difference in the size of divalent heterometal ions. Hence the ground- and excited-state properties are intrinsic to the $S = {}^5/_2$ $[Fe_3S_4]^-$ and $S = 2$ $[Fe_3S_4]^0$ fragments and the incorporation of Cd^{2+} rather Zn^{2+} is only manifest by a 230 mV decrease in the midpoint potential. While the $[CdFe_3S_4]^{2+,+}$ and $[ZnFe_3S_4]^{2+,+}$ clusters in *Da* FdIII have lower midpoint potentials than their *Pf* Fd counterparts ($E_m = -590$ mV *versus* −470 mV for the $[CdFe_3S_4]^{2+,+}$ couples and $E_m = -480$ mV *versus* −241 mV for the $[ZnFe_3S_4]^{2+,+}$ couples), a substantial decrease in potential for Cd compared to Zn is apparent in both proteins.

Heterometallic cubanes involving $[CuFe_3S_4]^{2+,+}$ cores were first reported in *Da* FdIII,[23] and comparison of the EPR, VTMCD, and redox properties for these clusters in *Pf* Fd and *Da* FdIII attests to analogous clusters in both proteins. In accord

(43) (a) Onate, Y. A.; Finnegan, M. G.; Hales, B. J.; Johnson, M. K. *Biochim. Biophys. Acta* **1993**, *1164*, 113−123. (b) Onate, Y. A.; Vollmer, S. J.; Switzer, R. L.; Johnson, M. K. *J. Biol. Chem.* **1989**, *264*, 18386−18391. (c) Flint, D. H.; Emptage, M. H.; Finnegan, M. G.; Fu, W.; Johnson, M. K. *J. Biol. Chem.* **1993**, *268*, 14732−14742. (d) Koehler, B. P.; Mukund, S.; Conover, R. C. Dhawan, I. K.; Roy, R.; Adams, M. W. W.; Johnson, M. K. *J. Am. Chem. Soc.* **1996**, *118*, 12391−12405.

with the analysis presented for *Da* FdIII,[23] the electronic, magnetic, and redox properties are indicative of Cu^+ bound with high affinity to $S = {}^1/_2$ $[Fe_3S_4]^+$ or $S = 2$ $[Fe_3S_4]^0$ cluster fragments. Only soft, monovalent transition metal ions such as Tl^+ and Cu^+ have been found capable of binding to the less nucleophilic tri-μ_2-sulfido face of a $[Fe_3S_4]^+$ cluster fragment,[23,27,28] and the smaller size of Cu^+ (radius 0.94 Å) compared to Tl^+ (radius 1.50 Å) presumably accounts for the much higher affinity for Cu^+. The only significant differences between the clusters in *Pf* Fd and *Da* FdIII lie in the observation of resolved ^{63,65}Cu hyperfine on the $S = {}^1/_2$ resonance from the $[CuFe_3S_4]^{2+}$ cluster in *Pf* Fd and a 40-mV increase in the midpoint potential for the $[CuFe_3S_4]^{2+,+}$ couple in *Pf* Fd ($E_m = -192$ mV for *Pf* Fd compared to $E_m = -148$ mV for *Da* FdIII). The latter is presumably a consequence of the cluster protein environment since the midpoint potentials of the known homometallic and heterometallic cubane clusters in *Da* FdIII are invariably lower (by 40−240 mV) than their *Pf* Fd counterparts. The observation of resolved ^{63,65}Cu hyperfine on the $g_{||}$ component of the $S = {}^1/_2$ $[CuFe_3S_4]^{2+}$ EPR signal ($a_{||} =$ 1.2 mT) provides unambiguous support for Cu incorporation and shows that the unpaired electron from the Fe−S fragment is partially delocalized onto the Cu atom. The extent of delocalization can be gauged by the observation that the hyperfine coupling constant is less than 20% of that encountered in oxidized blue copper proteins, in which the unpaired electron is substantially delocalized onto a single cysteinyl sulfur, and less than 7% of that found in aqueous Cu^{2+}.

Heterometallic cubanes involving $[CrFe_3S_4]$ cores have never before been synthesized in a Fd or in aprotic media. The EPR and VTMCD studies of the $[CrFe_3S_4]^{2+,+}$ clusters ($E_m = -440$ mV at pH 7.0) in *Pf* Fd reported herein indicate $S = 0$ and $S = {}^3/_2$ ground states for the oxidized and reduced forms, respectively. These spin states are analogous to those of the native $[Fe_4S_4]^{2+,+}$ cluster in *Pf* Fd, except that the $[Fe_4S_4]^+$ cluster is a mixed-spin system in frozen solutions with $S = {}^3/_2$ (80%) and $S = {}^1/_2$ (20%) ground states.[29] However, recent ^{1}H NMR studies indicate that the $S = {}^3/_2$ form is likely to be a freezing artifact since only the $S = {}^1/_2$ form is apparent at room temperature.[31] In contrast, the homogeneous $S = {}^3/_2$ ground state of synthetic and protein-bound $[NiFe_3S_4]^+$ clusters[21,44] is clearly not a freezing artifact, and the absence of any $S = {}^1/_2$ component for the $[CrFe_3S_4]^+$ cluster in *Pf* Fd suggests that the $S = {}^3/_2$ ground state is also an intrinsic property of this cluster. While both the $S = {}^3/_2$ $[Fe_4S_4]^+$ and $[NiFe_3S_4]^+$ clusters in *Pf* Fd exhibit similar rhombicities, $E/D = 0.22$ and 0.18, respectively,[21,29] compared to the dominant $S = {}^3/_2$ $[CrFe_3S_4]^+$ cluster, $E/D = 0.21$, these three clusters are readily distinguished by the sign and/or magnitude of their axial zero-field splitting parameters, $D = +3.3$, -2.2, and $+0.37$ cm^{-1} for $[Fe_4S_4]^+$,[29] $[NiFe_3S_4]^+$,[21] and $[CrFe_3S_4]^+$, respectively. Moreover, they each have distinctive excited-state properties as evidenced by their VTMCD spectra. The origin of the heterogeneity in the $S = {}^3/_2$ $[CrFe_3S_4]^+$ species ($E/D = 0.21$ and 0.10), which is apparent in the EPR data collected thus far, is unclear at present. However, it is interesting to note that similar changes in rhombicity are induced by exogenous ligand binding at the Ni site in the $[NiFe_3S_4]^+$ cluster.[21,22] This raises the possibility that the heterogeneity is a consequence of medium-dependent changes in ligation at the Cr site and EPR experiments as a function of the nature of medium in the presence and absence of exogenous ligands are currently in progress to address this issue.

Mössbauer studies have shown that ground-state spin of the $[Fe_3S_4]^0$ and $[Fe_3S_4]^-$ fragments results from antiferromagnetic interaction between a $S = {}^9/_2$ valence-delocalized $[Fe_2S_2]^+$ unit and a high-spin Fe^{2+} ($S = 2$) or Fe^{3+} ($S = {}^5/_2$) site.[26] Moreover, the ground- and excited-state properties of valence-delocalized $[Fe_2S_2]^+$ units have recently been established via EPR, VTMCD, and Mössbauer studies of Cys-to-Ser mutants of *Clostridium pasteurianum* 2Fe Fd.[45] Of particular importance to the present work is that VTMCD provides a convenient means of assessing the presence of a valence-delocalized $[Fe_2S_2]^+$ unit in higher nuclearity clusters via the presence of an intense positive band in the 700−800 nm region. This band is the hallmark of a valence-delocalized $[Fe_2S_2]^+$ unit and is attributed to the $\sigma \rightarrow \pi^*$ transition of the Fe−Fe interaction that is responsible for the spin-dependent valence delocalization. By this criterion, valence-delocalized $[Fe_2S_2]^+$ units associated with $[Fe_3S_4]^0$ or $[Fe_3S_4]^-$ fragments are present in the $[CdFe_3S_4]^{2+,+}$, $[CrFe_3S_4]^+$, and $[CuFe_3S_4]^+$ clusters investigated in this work but not the $[CuFe_3S_4]^{2+}$ cluster; cf. Figures 2, 5, and 10 with Figure 8. This is consistent with an idealized picture in which Cu^+ binds to a redox-active $[Fe_3S_4]^{+,0}$ fragment and Cr^{2+} or Cd^{2+} binds to a redox-active $[Fe_3S_4]^{0,-}$ fragment.

In previous work,[18] we have noted that the ground-state spin of heterometallic and homometallic cubanes ($[MFe_3S_4]^{2+,+}$, where M = Fe, Zn, Co, Ni, Mn, Tl) can be rationalized on the basis of antiferromagnetic coupling between the high-spin metal ion, M^{n+} with $n = 1$ or 2, and the appropriate cluster fragment, i.e. $[Fe_3S_4]^+$ ($S = {}^1/_2$), $[Fe_3S_4]^0$ ($S = 2$), or $[Fe_3S_4]^-$ ($S = {}^5/_2$). The underlying assumptions are localized valencies for the heterometal ion and the cluster fragment and that redox chemistry is confined exclusively to the Fe−S cluster fragment. While magnetic coupling is not required to explain the spin states of the $[CuFe_3S_4]^{2+,+}$ and $[CdFe_3S_4]^{2+,+}$ clusters due to the diamagnetism of the d^{10} Cu^+ and Cd^{2+} ions, the simple coupling scheme outlined above predicts $S = 0$ and ${}^1/_2$ ground states for the $[CrFe_3S_4]^{2+}$ and $[CrFe_3S_4]^+$ clusters, respectively, i.e. antiferromagnetic interaction between $S = 2$ Cr^{2+} ions and $S = 2$ $[Fe_3S_4]^0$ or $S = {}^5/_2$ $[Fe_3S_4]^-$ fragments. Hence, it is successful in rationalizing the observed $S = 0$ ground state of the $[CrFe_3S_4]^{2+}$ cluster but not the observed $S = {}^3/_2$ ground state of the $[CrFe_3S_4]^+$ cluster. Likewise the $S = {}^3/_2$ ground state of $[Fe_4S_4]^+$ clusters in native *Pf* Fd cannot be explained by this simple coupling scheme. While these $S = {}^3/_2$ spin states could be rationalized by invoking intermediate spin states, $S = 1$, for five-coordinate localized-valence Fe^{2+} or Cr^{2+} ions with bidentate aspartate coordination, the trends in midpoint potentials as a function of the heterometal and the available Mössbauer data indicate that the underlying assumptions of this approach are not always valid.

The trend in the midpoint potentials of $[MFe_3S_4]^{2+,+}$ clusters in *Pf* Fd as a function of the heterometal M is depicted in Figure 11. In light of the redox inertness of Zn^{2+}, it is appropriate to evaluate the midpoint potential of these clusters relative to that of the $[ZnFe_3S_4]^{2+,+}$ couple, since this provides the best measure of the intrinsic potential of the $[Fe_3S_4]^{0,-}$ fragment in a cubane cluster. Clusters with higher midpoint potentials require het-

(44) (a) Ciurli, S.; Yu, S.-B.; Holm, R. H.; Srivastava, K. K. P.; Münck, E. *J. Am. Chem. Soc.* **1990**, *112*, 8169−8171. (b) Zhou, J.; Scott, M. J.; Hu, Z.; Peng, G.; Münck, E.; Holm, R. H. *J. Am. Chem. Soc.* **1992**, *114*, 10843−10854.

(45) (a) Crouse, B. R.; Meyer, J.; Johnson, M. K. *J. Am. Chem. Soc.***1995**, *117*, 9612−9613. (b) Achim, C.; Golinelli, M. P.; Bominaar, E. L.; Meyer, J.; Münck, E. *J. Am. Chem. Soc.* **1996**, *118*, 8168−8169. (c) Johnson, M. K.; Duin, E. C.; Crouse, B. R.; Golinelli, M.-P.; Meyer, J. In *Spectroscopic Methods in Bioinorganic Chemistry*; Solomon, E. I., Hodgson, K. O., Eds.; ACS Symposium Series; American Chemical Society: Washington, DC, in press.

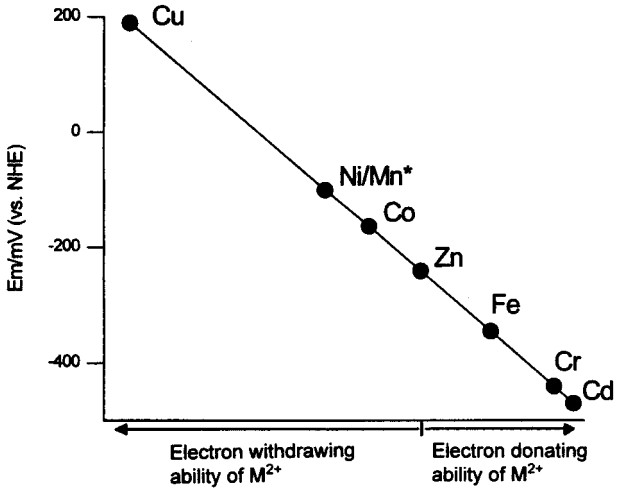

Figure 11. Pictorial representation of the observed trend in the midpoint potentials of $[MFe_3S_4]^{2+,+}$ as a function of the heterometal M. Asterisk indicates only lower limits are available for the midpoint potentials of $[NiFe_3S_4]^{2+,+}$ and $[MnFe_3S_4]^{2+,+}$, since oxidation at higher potentials leads to loss of the heterometallic ion and the formation of $[Fe_3S_4]^{+,0}$ clusters.

erometal sites that are capable of reduction over the physiological potential range (i.e. accessible $M^{2+,+}$ couples), thereby minimizing the negative charge on the Fe−S fragment. Cu provides the extreme example, and the spectroscopic properties are clearly most consistent with almost complete transfer of an electron in both redox states, resulting in a bound Cu^+ ion. The midpoint potential of the $[CuFe_3S_4]^{2+,+}$ couple therefore provides an estimate for the midpoint potential of a $[Fe_3S_4]^{+,0}$ cluster fragment in a cubane cluster. Partial transfer of negative charge from the Fe−S cluster fragment onto the heterometal has been invoked to explain the average Fe isomer shifts of the $[CoFe_3S_4]^+$ and $[NiFe_3S_4]^+$ clusters,[19,22,46] indicating formal oxidation states between +1 and +2 for the Co and Ni ions. Clusters with lower midpoint potentials relative to the $[ZnFe_3S_4]^{2+,+}$ couple require heterometal sites such as Fe and Cr that are only capable of oxidation over the physiological potential range (i.e. accessible $M^{2+,3+}$ couples) or are electron rich as in the case of Cd^{2+}. While additional Mössbauer studies are required for detailed assessment of the electron distributions, it seems likely that the $[MFe_3S_4]^{2+,+}$ midpoint potential provides a reliable indicator of the charge distribution between the heterometal and Fe−S cluster fragment.

Acknowledgment. This work was supported by a grant from the National Institutes of Health (GM45597 to M.W.W.A. and M.K.J.) and by a National Science Foundation Research Training Grant Award to the Center for Metalloenzyme Studies (BIR-9413236).

IC970200K

(46) Cen, W.; Lee, S. C.; Li, J.; MacDonnell, F. M.; Holm, R. H. *J. Am. Chem. Soc.* **1993**, *115*, 9515−9523.